Journal of Engineering Sciences
Vol 11, Issue 5,May/2020
ISSN NO:0377-9254

Fuzzified Single Stage PV Array Fed Speed Sensorless Vector Control of Induction Motor Drive for Water Pumping

[1] Amrutha Bharati, [2] Manaswini Ashok Kamtam, [3] M K Revanth [4] Sri ram Ramu (MTech (Ph.D) Associate Professor)
Sreenidhi Institute Of Science And Technology, Yamnampet, Rangareddy district, **Telangana.**
[1]amruthabharati4@gmail.com,, 2manaswinikamtam@gmail.com , [3]revanthmandula0066@gmail.com, [4]ramu_sriram@yahoo.co.in

Abstract— ***This paper deals with a single stage solar powered speed sensorless vector controlled induction motor drive for water pumping system by using fuzzy logic controller The proposed system includes solar photovoltaic (PV) array, a three-phase voltage source inverter (VSI) and a motor-pump assembly. An incremental conductance (***INC***) based MPPT (Maximum Power Point Tracking) algorithm is used to harness maximum power from a PV array. The smooth starting of the motor is attained by vector control of an induction motor. Results were compared to classify the difference between Conventional (PI) and Proposed (FLC.)The desired configuration is designed and simulated in MATLAB/Simulink platform and the design, modeling and control of the system, are validated on an experimental prototype developed in the laboratory***.

Keywords- *Field-Oriented Vector Control (FOC), Photovoltaic (PV), INCMPPT Algorithm, Induction Motor Drive (IMD), Water Pump.*

I. INTRODUCTION

In the modern era of development, renewable resources of energy, are being advocated by many countries to meet the increasing demand of electrical energy due to rapid depletion of non-renewable resources [1]-[2]. Solar PV based energy generation, has come up as an important alternative for many purposes [3]. The irrigation sector is one of the major sectors where solar PV power is extensively used for water pumping [4-5]. Solar PV water pumping has been initially realized using the DC motor. However, with all due virtues associated with the induction motor in terms of mechanical simplicity, ruggedness, reliability, low cost, higher efficiency and lower maintenance than the DC motors, it has replaced DC motors. Here, a solar PV array fed induction motor drive using vector control is used [6]-[7],as one knows that solar PV power depends on solar insolation and temperature. The characteristic of PV module exhibits a single power peak. An extraction of maximum power is very important part of the PV system. Therefore, various MPPT (Maximum Power Point tracking) techniques have been developed and explained in the literature. These algorithms vary in their speed, range of effectiveness and complexities [8]. Here, an incremental conductance (InC) based MPPT algorithm is used to track MPPT. This algorithm is developed to overcome some drawbacks of perturb and observe (P&O) algorithm. INC algorithm improves the tracking time and to produce increased energy on a vast irradiation changes. Moreover, it has advantage over P&O method, which increases losses in slow varying atmospheric condition as it oscillates around MPP [9]-[10].

Most of the existing induction motor drives (IMDs) incorporate one DC-DC converter and a VSI (Voltage Source Inverter) for achieving MPPT and maximum efficiency of the motor [11]. Moreover, the DC link voltage regulation is achieved by VSI itself. However, the system requires at least seven power converter switches and hence switching losses are increased. This further includes a DC-AC conversion with a VSI feeding a vector-controlled three-phase IMD. Therefore, there is a need to use single stage controlled drive for water pumping and thereby decreasing number of switches and losses. In single stage system, a VSI has to maintain the MPP as well as DC link voltage is also controlled by it. Therefore, variable DC link voltage cannot be achieved as explained in [12]-[13]. The vector control strategy is superior to scalar control in terms of speed of response and accuracy as explained in [14]- [16]. In the vector

control technique, an AC motor is operated in such a manner to behave dynamically as a DC motor by using feedback control [16]. This technique enables to vary the speed over the wide range. Hence with the advancement of power electronics and by using powerful microcomputer and DSPs, the vector control ousts scalar control [17]-[19]. In this vector control scheme, the stator flux is estimated in stationery αβ frame, which is used to estimate the slip speed (ωsl), synchronous speed (ωe) and the motor speed as explained in [20]. The paper is organized as given: system configuration is given in section II followed by the design of system, control strategy including vector control and results and discussion in the subsequent sections. The performance of the given system is achieved through simulation using MATLAB/Simulink. Simulation results are validated by experimentation carried out in the laboratory on the developed prototype.

II. SYSTEM CONFIGURATION

Fig.1 shows the configuration of a single stage solar PV array fed speed senseless induction motor drive incorporating vector control for water pumping. This proposed system constitutes PV array followed by a VSI fed three-phase induction motor drive operated pump. The motor speed is estimated by stator fluxes, which is estimated by DC link voltage and motor currents. Three-phase VSI switching is controlled by hysteresis-band controller. An incremental conductance (INC) control algorithm is used for MPPT to generate switching pulses for the VSI.

III. SYSTEM DESIGN

Fig.1 shows a basic schematic of a three-phase induction motor of a 7.5 kW (10 HP), 415V, used to drive the pump powered by a 8.7 kW maximum power solar PV array. The various stages of system have been designed here and the performance of overall system is shown in subsequent sections under various conditions. The detailed data are given in Appendices.

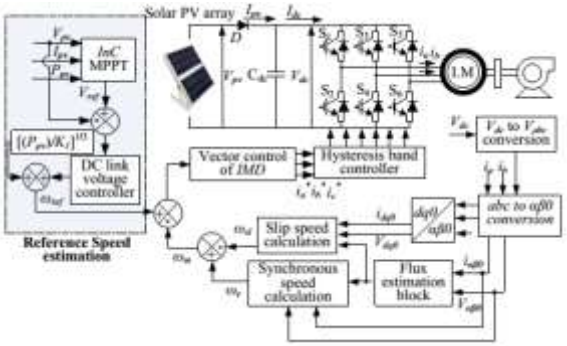

Fig. 1. PV fed induction motor drive configuration

A.Design of Solar PV Array

A 8700 W PV array is designed to drive a 7.5kW induction motor drive. The rating of PV array is selected more than the motor rating so that the performance of the motor remains unaffected by the losses incurred in the motor and converter. A PV array is designed by connecting 34 PV modules in series of open circuit voltage (Voc) equals 734V and 25 modules in parallel of short circuit current (Isc) equal to 15.5 A, respectively. The voltage and current reach their MPP on about 81% of V oc and 90% of Isc respectively as given in Table I. The specifications of PV module used, are given in Table II and in Appendices

TABLE I PV ARRAY DESIGN (SIMULATION DATA)

MPP voltage, V_{mp}	600V
MPP power, P_{mp}	8700W
MPP current, $I_{mp}= P_{mp}/V_{mp}$	14.5A
Number of module in series, $N_{ss}= V_{mp}/V_{mpp}$	34
Number of module in parallel, $N_{pp}=I_{mp}/I_{mpp}$	25

TABLE II PV MODULE (SIMULATION DATA)

V_{oc} of one module	21.6V
I_{sc} of one module	0.64A
MPP Voltage, V_{mpp}	0.81*21.6=17.6V
MPP Current, I_{mpp}	0.9*0.64=0.58A

B. Calculation of DC Link Voltage

In order to control the output current of VSI, the voltage of the DC link should be more than as compared to the peak amplitude of line voltage given to the motor [13].

$$V_{dc} = \sqrt{2}*V_L=\sqrt{2}*415=587V \quad \text{.....(1)}$$

Hence the value of DC link voltage is kept as 600V.

C. Design of DC Link Capacitor

The value of DC link capacitor is estimated by using fundamental frequency component as [13],

$\omega_{rated} = 2 * \pi * f_{rated}$=2*π*50=314 rad/s….(2)

$\frac{1}{2} * C_{dc} * \left({v_{dc}}^2 - {V_{dc}}^2\right) =$
$3aV_pIt$=3*1.2*239.6*13.5*0.005……(3)

Hence, C_{dc}= 2509µF

Where V_{dc} is the DC link voltage and Vdc1 is the minimum allowable DC link voltage during transient condition, t is the time required for the voltage to recover minimum allowable DC-link voltage, I is the motor phase current and V_p is the phase voltage. Therefore, capacitor value is selected as 2500 µF.

D. Design of Water Pump

Water pumps have non-linear relationship between load torque and motor speed [21] i.e. load torque (TL) is directly in proportion to the square of the rated rotor speed. Hence,

$$T_L = K_1 {\omega^2}_m \text{ ……(4)}$$

Where K_1 is the proportionality constant of the pump.

IV. CONTROL OF RECOMMENDED SYSTEM

The control of overall system includes MPPT of solar PV array to extract maximum power through three phase VSI, control of three-phase VSI switching by using hysteresis-band controller for vector-controlled IMD and speed estimation for speed sensorless vector control of an induction motor drive.

A. Incremental-Conductance Algorithm

The technique for controlling the PV array voltage is given in Fig.2. There is a nonlinear relationship between power and voltage in solar PV array characteristic and various MPPT techniques have been used to track maximum power point. However, because of its inherent demerit of oscillation at MPP and loss associated with P&O technique as discussed in previous section, an INCcontrol algorithm is used. The commanding equations for explaining the operating principle of InC, are given as,

$$P_{pv} = V_{pv} * I_{pv} \text{…… (5)}$$

$$\frac{\Delta P_{pv}}{\Delta V_{pv}} = I_{pv} + V_{pv} * \frac{\Delta P_{pv}}{\Delta V_{pv}} = 0 \text{…….. (6)}$$

$$\frac{\Delta I_{pv}}{\Delta V_{pv}} = -\frac{I_{pv}}{V_{pv}} \text{…….. (7)}$$

Where V_{pv} and I_{pv} are the instantaneous voltage and current values. The reference voltage V_{ref} is bonded between upper and lower limit set between 0.9V oc-0.8Voc. In case, if V_{ref} does not lie within the boundary, it is set to its nearest saturated value. From the above equation, it is clear that on the left side of MPP the slope is positive meaning $\Delta I_{pv}/\Delta V_{pv} > (-I_{pv}/V_{pv})$ and on the right side of MPP the slope is negative, which implies $\Delta I_{pv}/\Delta V_{pv} < (-I_{pv}/V_{pv})$ and slope at MPP should be zero as shown in Fig.2.

Fig.3 shows the method of perturbation using INCbased MPP algorithm.

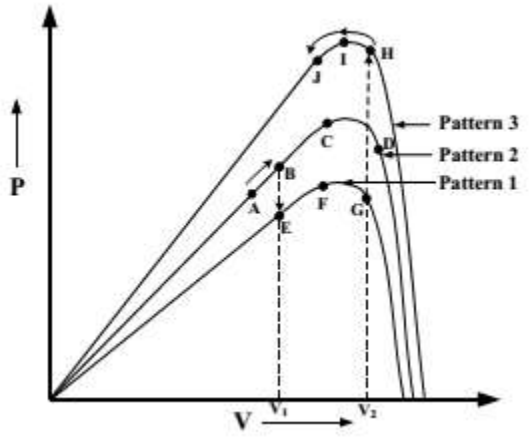

Fig. 2. Ppv-Vpv curve for one module

The inputs to the MPPT algorithm, are PV voltage and current. The reference PV voltage, thus obtained at kth sampling instant, is the reference DC link voltage Vdc* and it is compared with the PV voltage as,

$$V_{dcl(k)} = {V^*}_{dc(k)} - V_{pv(k)} \quad (8)$$

Fig.4 (a) shows the schematic for the generation of error signal $V_{dcl(k)}$, which is fed to DC link voltage PI controller and the resulting speed error signal at the k_{th} sampling instant and is given as follows,

$$\omega_{l(k)} = \omega_{l(k-1)} + K_{pdc}\{V_{dcl(k)} - V_{dcl(k-1)}\} + K_{idc}V_{dcl(k)} \ldots\ldots (9)$$

Fig.4 (b) shows the PV power converted into a speed term by the following relation and this gives one component of the reference speed by affinity law of pump. It can be treated as the feed forward component.

The physical significance of ω2 quantity can be justified as maximum rated speed corresponding to the given insolation. Only PI controller pushes the voltage error to the desired reference speed (ω_{ref}). However, the dynamic response of the system becomes very poor. It can be seen from the feed forward term that it consists of P_{pv} and the proportionality constant obtained from motor affinity law. Both of these terms help in fast dynamic response by instantaneously reflecting the PV power on motor speed. It is expressed by the following formula.

$$P_{pv} = K_1\omega^3{}_2 \ldots (10)$$

Where K_1 is proportionality constant of pump obtained in (4). Hence, the reference speed of the motor is estimated as,

$$\omega_{ref} = \omega_1 + \omega_2 \ldots\ldots (11)$$

This reference speed is used for control of VSI feeding induction motor drive.

TABLE-III MPPT THROUGH INCALGORITHM DURING INSOLATION VARIATION

Atmospheric condition	Current Point → Next point	Electrical quantity	Duty cycle
Fixed Solar Insolation (Pattern 2)	A→B	P↑ V↑	$V_{dc}^{*}+\Delta V_{pv}$
	B→C	P↑ V↑	$V_{dc}^{*}+\Delta V_{pv}$
	C→D	P↓ V↑	$V_{dc}^{*}+\Delta V_{pv}$
	D→C	P↑ V↓	$V_{dc}^{*}-\Delta V_{pv}$
	C→B	P↓ V↓	$V_{dc}^{*}-\Delta V_{pv}$
At point 'B', insolation changed New operating point is 'E'			
New Insolation level (Pattern 1)	E→F	P↑ V↑	$V_{dc}^{*}+\Delta V_{pv}$
	F→G	P↓ V↑	$V_{dc}^{*}+\Delta V_{pv}$
	G→F	P↑ V↓	$V_{dc}^{*}-\Delta V_{pv}$
	F→E	P↓ V↓	$V_{dc}^{*}-\Delta V_{pv}$
	E→F	P↑ V↑	$V_{dc}^{*}+\Delta V_{pv}$
	F→G	P↓ V↑	$V_{dc}^{*}+\Delta V_{pv}$
At point 'G', insolation changed New operating point is 'H'			
New Insolation level (Pattern 3)	H→I	P↑ V↓	$V_{dc}^{*}-\Delta V_{pv}$
	I→J	P↓ V↓	$V_{dc}^{*}-\Delta V_{pv}$
	J→I	P↑ V↑	$V_{dc}^{*}+\Delta V_{pv}$
	I→H	P↓ V↑	$V_{dc}^{*}+\Delta V_{pv}$

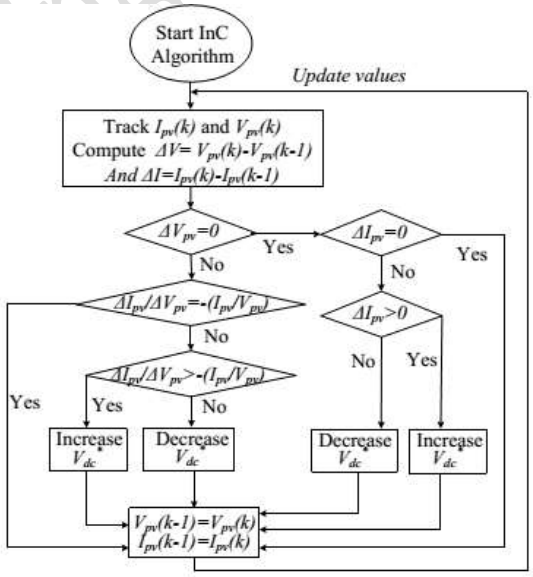

Fig. 3. Incremental-Conductance algorithm

B. Speed Estimation of Induction Motor Drive

The fundamental equations for the estimation of speed are given as follows.

The three phase VSI voltages (va, vb, vc) are obtained by the DC link voltage (Vdc) by the expression as,

$$V_a = \frac{V_{dc}}{3} * (2S_a - S_b - S_c),$$

$$V_b = \frac{V_{dc}}{3} * (2S_b - S_a - S_c)$$

$$V_c = \frac{V_{dc}}{3} * (2S_c - S_b - S_a) \ldots\ldots \quad (12)$$

Where S a, Sb and Sc are switching functions (which are either one or zero) of VSI.
The various voltage and current transformation equations to transform from abc to αβ domain are given as,

$V_a = \frac{1}{3}(2v_a - v_b - v_c), V_\beta = \sqrt{3}(v_b - v_c) \ldots$ (13)

$i_a = \frac{1}{3}(2i - i_b - i_c), i_\beta = \sqrt{3}(i_b - i_c) \ldots..$ (14)

Where i_a, i_b, i_c are balanced three phase winding currents

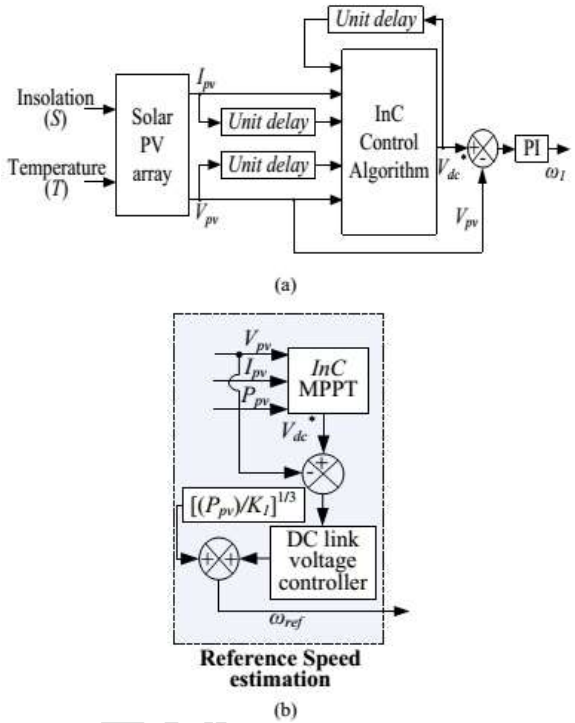

Fig. 4. Reference speed generation (a) ω1 estimation (b) Feed-forward speed component

This transformation is applicable for all rotating variables viz. voltage, current and flux quantities. The stationery components of flux are given as,

$$\frac{d}{dt}(\varphi_\beta) = (v_\beta - R_s * i_\beta), \frac{d}{dt}(\varphi_\alpha) = (v_\alpha - R_s * i_\alpha) \quad (15)$$

$$\varphi_s = \sqrt{\varphi_\alpha^2 + \varphi_\beta^2} \quad (16)$$

$$i_{qs} = i_\beta \times \frac{\varphi_\alpha}{\varphi_s} - i_\alpha \times \frac{\varphi_\beta}{\varphi_s} \quad (17)$$

$$i_{ds} = i_\beta \times \left({}^{\varphi_\beta}/_{\varphi_s}\right) + i_\alpha \times \left(\frac{\varphi_\alpha}{\varphi_s}\right) \quad (18)$$

$$\varphi_{ds} = \varphi_\beta \times \left(\frac{\varphi_\beta}{\varphi_s}\right) + \varphi_\alpha \times \left({}^{\varphi_\alpha}/_{\varphi_s}\right) \quad (19)$$

$$w_c = \frac{(V_\beta - R_s * i_\beta)\varphi_\alpha - (V_\alpha - R_s * i_\alpha)\varphi_\beta}{\varphi^2} \quad (20)$$

Where ids and iqs are current components in synchronously rotating dq0 frame,

$$\sigma = 1 - \frac{L_m^2}{(L_s * L_r)}, \qquad \tau_r = L_r/R_r \ ,$$

Lr=rotor inductance, Lm=magnetizing inductance, Llr= rotor leakage inductance, Lls= stator leakage inductance, Rr=stator referred rotor resistance, Rs=stator resistance.

The motor rotational speed is given as,

$$\omega_m = \omega_e - \omega_{sl} \quad (21)$$

The slip speed (ωsl) and synchronous speed (ωe) are estimated as,

$$\omega_{sl} = \frac{(1 + \sigma S\tau_r)L_s i_{qs}}{\tau_r(\varphi_d - \sigma L_s i_{ds})} \quad (22)$$

C. Field-Weakening Control

The relationship of direct axis current with speed (ω_m) at a given base speed of the motor (ωbase) is given below,

$$I_{dm}^{e^*} = I_{mag} \quad (for\ \omega_m \le \omega_{base}) \quad (23)$$

$$I_{dm}^{e^*} = \frac{\omega_{base}}{\omega_m} I_{mag} \quad (for\ \omega_m > \omega_{base}) \quad (24)$$

Where I mag is the magnetizing current of the motor.

D. Vector Control of Induction Motor Drive

Fig.5 shows the schematic of vector control method, which is used to control the stator currents and flux. It comprises of three stages.

The flux component of current vector (Idm*) is calculated as,

$$I_{dm}^{*} = I_{dm}^{e^{*}} + \tau_r \times \frac{d}{dt} I_{dm}^{e^{*}} \qquad (25)$$

During steady-state condition, the derivative term tends to zero.

The reference flux component (ψds*) is calculated as,

$$\psi_{ds}^{*} = L_m I_{dm}^{e^{*}} \qquad (26)$$

The flux error is passed through flux PI controller, which pushes the error signal to zero and the output is the exciting current (Ids*). The involved equations are given as,

$$\psi_e = \psi_{ds}^{*} - \psi_{ds} \qquad (27)$$

$$I_{ds(k)}^{*} = I_{ds(k-1)}^{*} + K_{ds}\{\psi_{e(k)} - \psi_{e(k-1)}\} + K_{iv}\psi_{e(k)} \qquad (28)$$

Some decoupling effect is present in vector control, due to which the change is torque component of current (iqs) can change the torque as well as flux. Therefore, this effect must be eliminated by adding one feed-forward path. The equation of decoupling component of current is given as,

$$I_{dcp} = \frac{\sigma \tau_r \omega_{sl} i_{qs}}{1 + \sigma S \tau_r}$$

Therefore, the final expression for exciting component of current is given as,

$$I_{ds}^{e^{*}} = I_{ds}^{*} + I_{dcp} \qquad (30)$$

The torque component of current vector (Iqse*) is calculated as follows,

The desired speed (ωref) and estimated speed (ωm) is compared and the error is passed through speed PI controller to generate reference torque (Te(k)*) as,

$$\omega_{error} = \omega_{ref} - \omega_m \qquad (31)$$

$$T_{e(k)}^{*} = T_{e(k-1)}^{*} + K_{p\omega}\{\omega_{error(k)} - \omega_{error(k-1)}\} + K_{i\omega}\omega_{error(k)} \qquad (32)$$

$$I_{qs}^{e^{*}} = \frac{T_e^{*}}{K \times I_{ds}^{e^{*}}} \qquad (33)$$

Where K=3PLm/4Lr,P is the number of poles.

The reference slip speed (ωsl*) is calculated as,

$$\omega_{sl}^{*} = I_{qs}^{e^{*}} / \left(\tau_r * I_{ds}^{e^{*}}\right) \qquad (34)$$

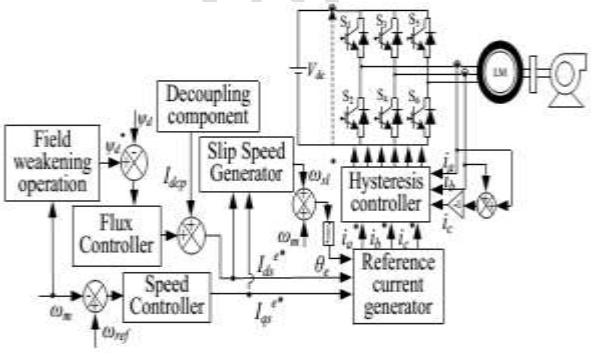

Fig. 5. Vector control of IMD

This reference slip speed (ωsl*) is added with the estimated speed (ωm) to calculate reference synchronous speed (ωe*) in rad/s.

$$\omega_e^{*} = \omega_m + \omega_{sl}^{*} \qquad (35)$$

The synchronous speed thus calculated is used to get flux-angle (θe) at the kth sampling instant as,The synchronous speed thus calculated is used to get flux-angle (θe) at the kth sampling instant as,

$$\theta_{e(k)} = \theta_{e(k-1)} + \omega_e^{*} \times T \qquad (36)$$

where T=Sampling period of the signal. The value of q-axis and d-axis current components Idse* and I qs e* respectively obtained from (30) and (33), are used to obtain reference phase currents ia*, ib*, ic*, by following equations,

$$i_a^* = I_{ds}^{e*}\sin\theta_e + I_{qs}^{e*}\cos\theta_e \quad (37)$$

$$i_b^* = I_{ds}^{e*}\sin\left(\theta_e - 120^\circ\right) + I_{qs}^{e*}\cos\left(\theta_e - 120^\circ\right) \quad (38)$$

$$i_c^* = I_{ds}^{e*}\sin\left(\theta_e + 120^\circ\right) + I_{qs}^{e*}\cos\left(\theta_e + 120^\circ\right) \quad (39)$$

These phase currents (ia*, ib*, ic*) are compared with the sensed phase currents (ia, ib, ic) and the error signal is passed through hysteresis-band controller to generate switching pulses for VSI.

FUZZY LOGIC CONTROLLER

Fuzzy logic is applied with great success in various control application. Almost all the consumer products have fuzzy control. Some of the examples include controlling your room temperature with the help of air-conditioner, anti-braking system used in vehicles, control on traffic lights, washing machines, large economic systems, etc.

A control system is an arrangement of physical components designed to alter another physical system so that this system exhibits certain desired characteristics. Following are some reasons of using Fuzzy Logic in Control Systems

- While applying traditional control, one needs to know about the model and the objective function formulated in precise terms. This makes it very difficult to apply in many cases.
- By applying fuzzy logic for control we can utilize the human expertise and experience for designing a controller.
- The fuzzy control rules, basically the IF-THEN rules, can be best utilized in designing a controller.

Followings are the major components of the FLC as shown in the above figure –

Fuzzifier − the role of fuzzifier is to convert the crisp input values into fuzzy values.

Fuzzy Knowledge Base − It stores the knowledge about all the input-output fuzzy relationships. It also has the membership function which defines the input variables to the fuzzy rule base and the output variables to the plant under control.

Fuzzy Rule Base − It stores the knowledge about the operation of the process of domain.

Inference Engine − It acts as a kernel of any FLC. Basically it simulates human decisions by performing approximate reasoning.

Defuzzifier − the role of defuzzifier is to convert the fuzzy values into crisp values getting from fuzzy inference engine.

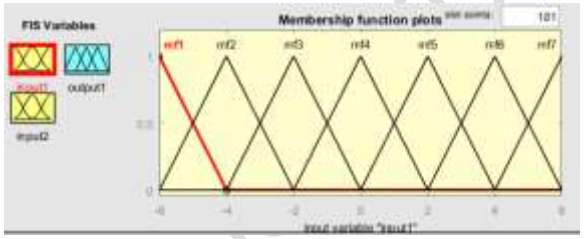

Fig.6 Shows the Membership functions for error.

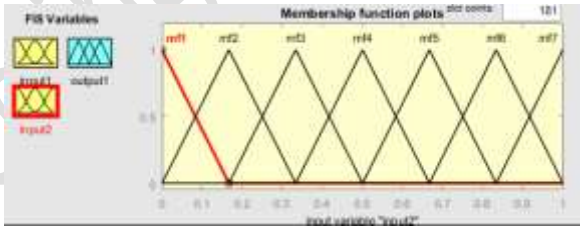

Fig.6 Shows the Membership function for Differentiated-error.

RESULTS AND DISCUSSION:

Performance at Constant Irradiance:

PI-CONTROLLER:

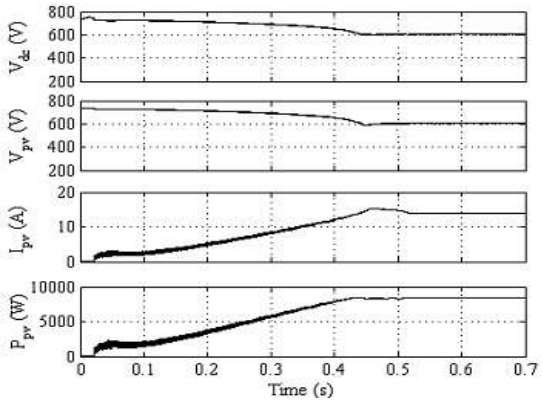

Fig.7 Shows the MPPT of PV array at 1000w/m^2

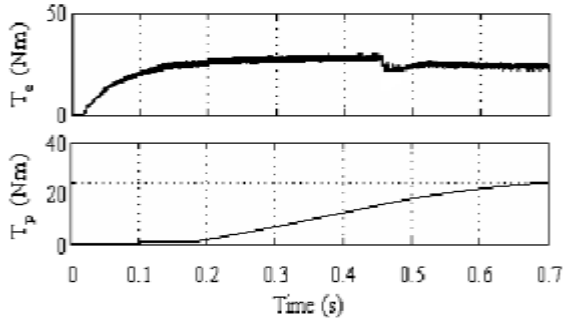

Fig.8 Shows the Electromagnetic torque and Estimate speed.

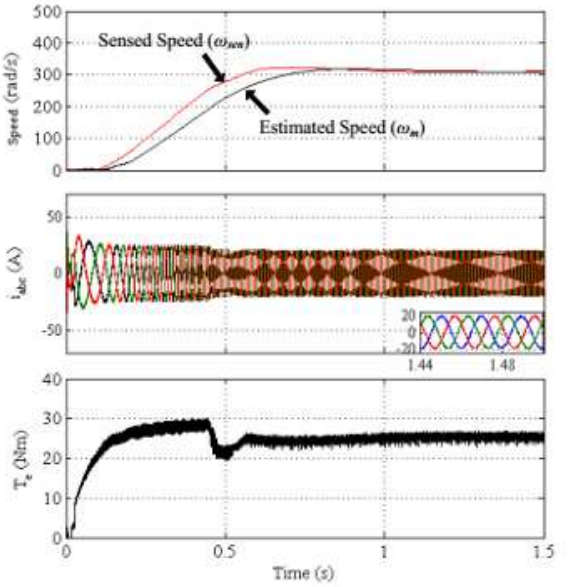

Fig.9 Shows the Speed parameters, Current and Electromagnetic Torque.

FUZZY-CONTROLLER:

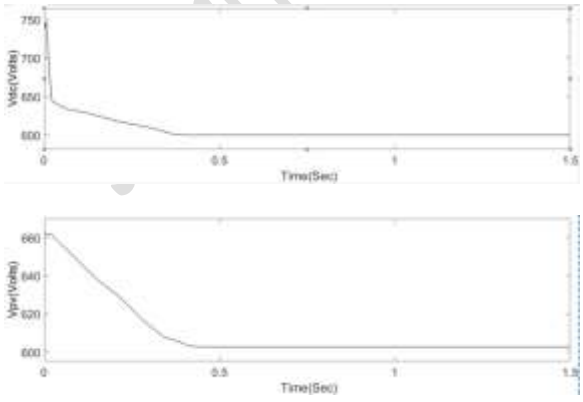

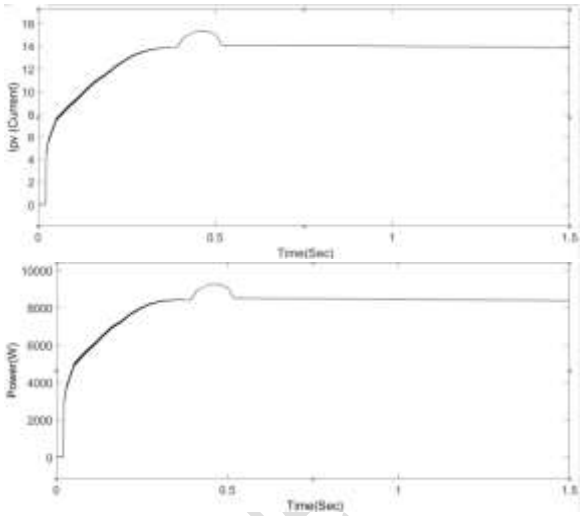

Fig.10 Shows the PV characteristics for Fuzzy Controller.

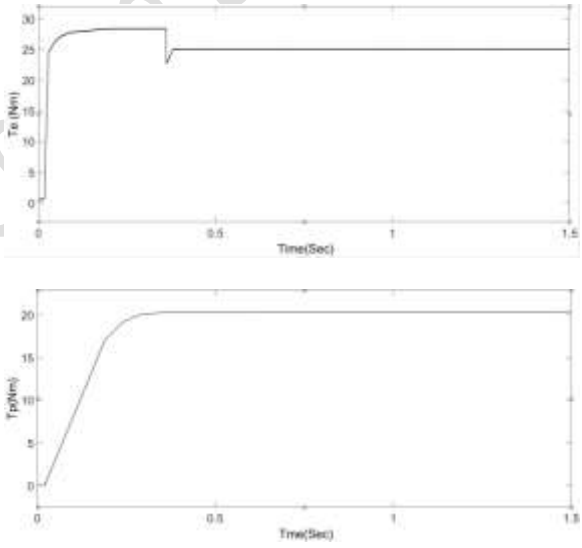

Fig.11 Shows the Electromagnetic torque and Estimate speed.

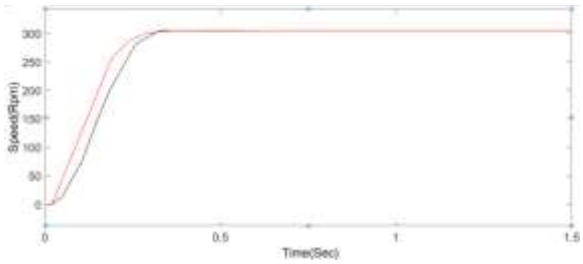

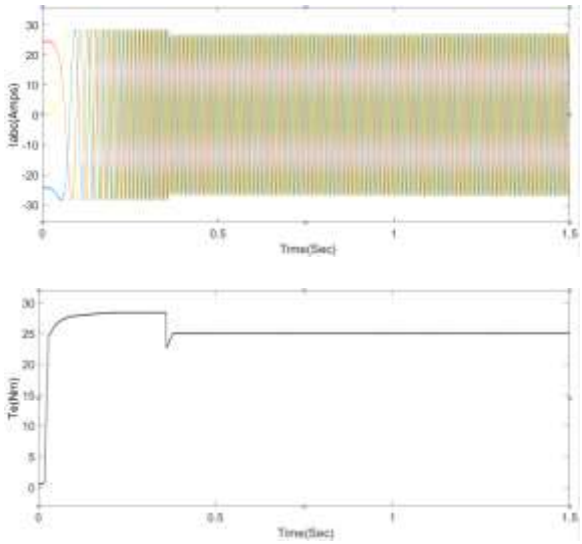

Fig.12 Shows the Speed parameters, Current and Electromagnetic Torque.

REDUCING IRRADIANCE:

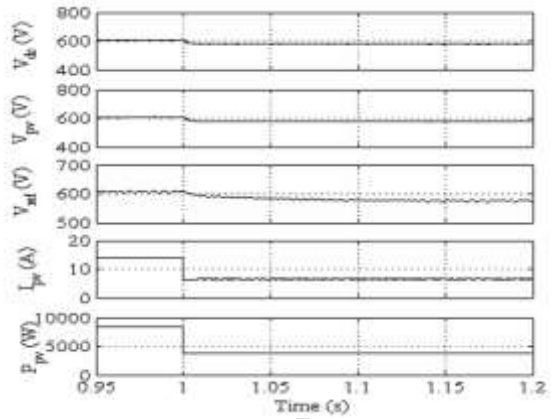

Fig.11 Shows the SPV array performance during decrease in irradiance from 1000 W/m2 to 500 W/m$^{2.}$

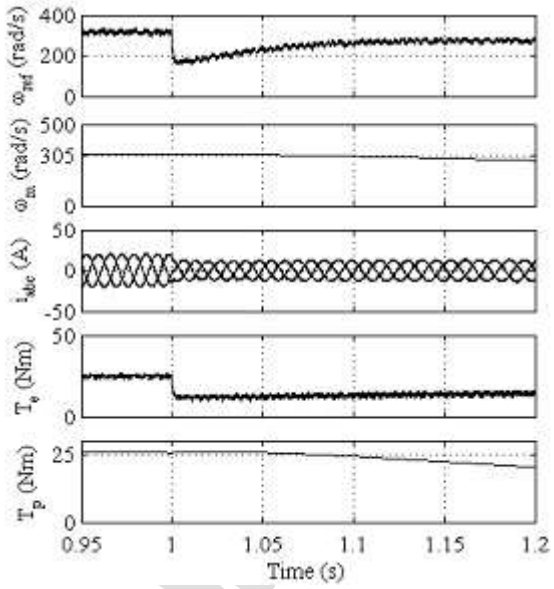

Fig12. Dynamic performance during irradiance decrement from 1000 W/m2 to 500 W/m2

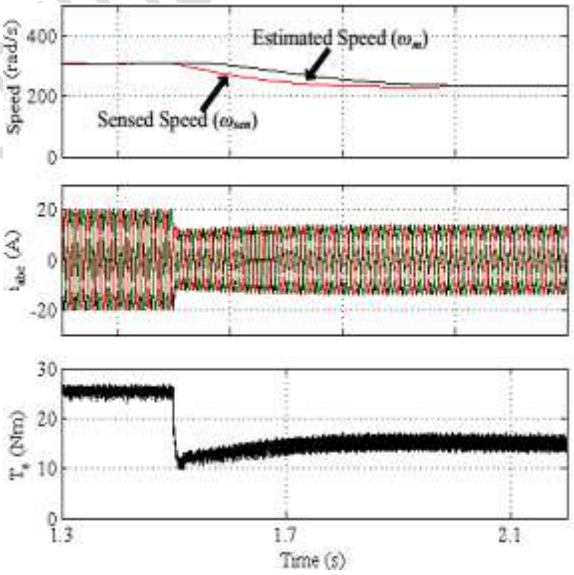

Fig.13 Shows the Speed parameters, Current and Electromagnetic Torque

FUZZY-LOGIC CONTROLLER:

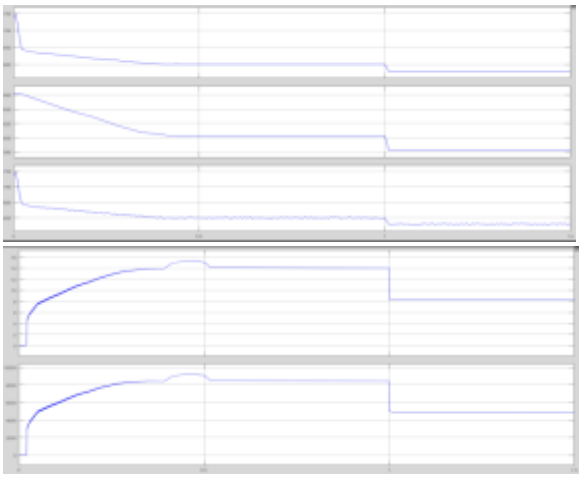

Fig.14 Shows the SPV array performance during decrease in irradiance from 1000 W/m2 to 500 W/m$^{2.}$

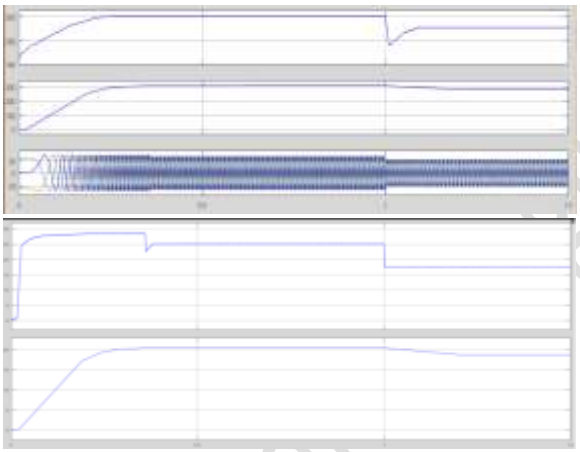

Fig15. Dynamic performance during irradiance decrement from 1000 W/m2 to 500 W/m2.

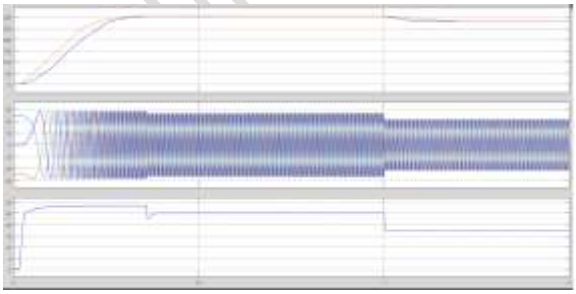

Fig.16 Shows the Speed parameters, Current and Electromagnetic Torque.

It is observed that the flux signals vary in their frequency as the irradiance is altered from 1000 W/m2 to 500 W/m2.

INCRESING IRRADIANCE:

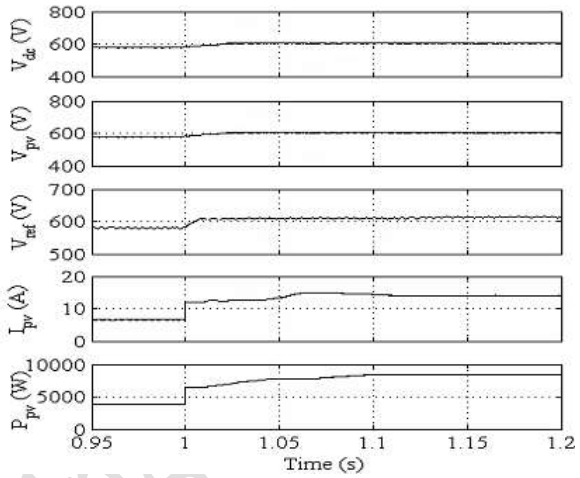

Fig.17 Shows the SPV array performance during increases in irradiance from 500 W/m2 to 1000 W/m$^{2.}$

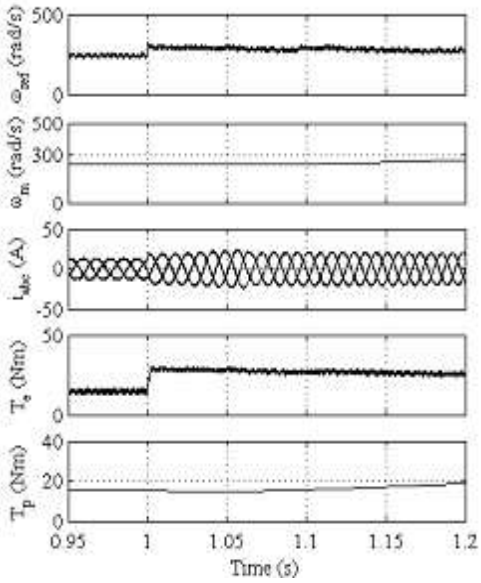

Fig18. Dynamic performance during irradiance increasing from 500 W/m2 to 1000 W/m2

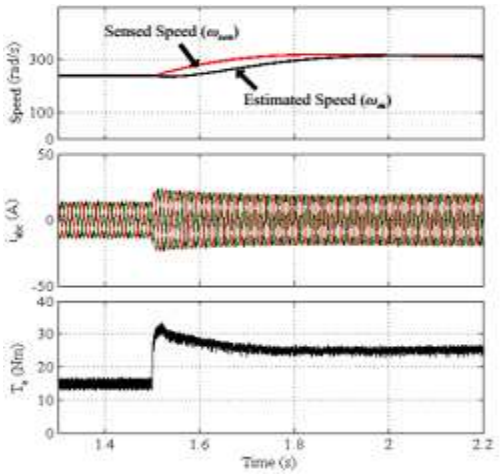

Fig.19 Shows the Speed parameters, Current and Electromagnetic Torque.

FUZZY LOGIC CONTROLLER:

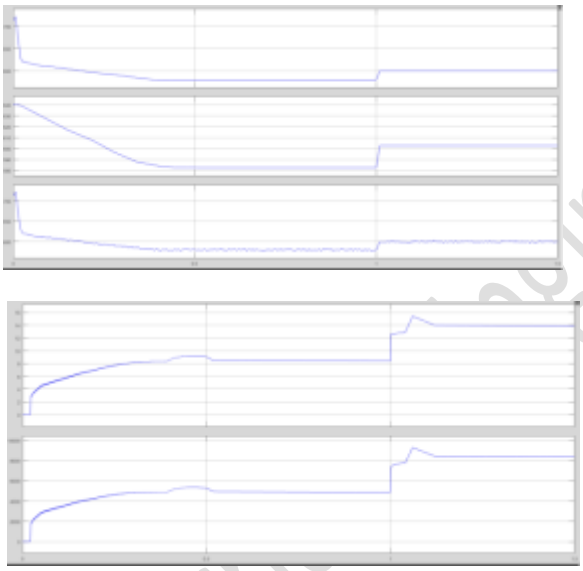

Fig.20 Shows the SPV array performance during increases in irradiance from 500 W/m2 to 1000 W/$m^{2.}$

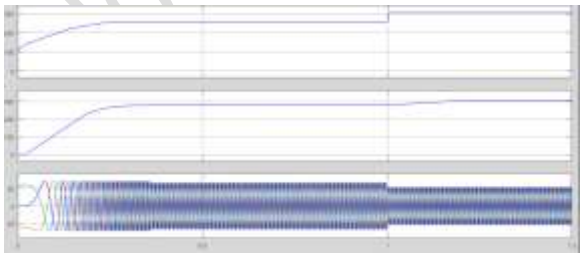

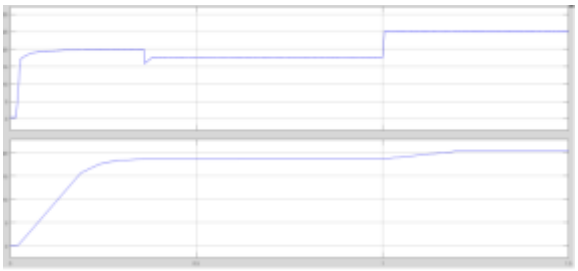

Fig21. Dynamic performance during irradiance increasing from 500 W/m2 to 1000 W/m2

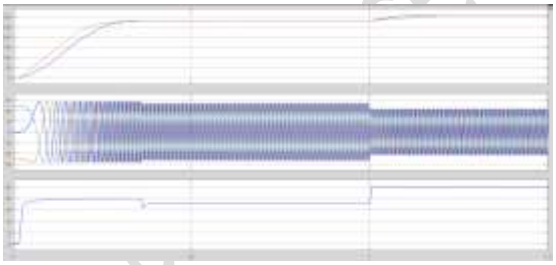

Fig.22 Shows the Speed parameters, Current and Electromagnetic Torque

In all cases, PV voltage and power shows the differences across the circuits. As Fuzzy is able to reduce the error more accurately, Proposed topology is showing results accurately. For the Torque calculations. Fuzzified concept is having fewer harmonic (Oscillations) than Conventional topology.

For speed controlling, Conventional reference speed and measured speed is having huge differences, whereas proposed topology is showing less variations.

CONCLUSION

A single stage solar PV array fed speed sensorless vector controlled induction motor drive has been operated subjected to different conditions and the steady state and dynamic behaviors with Fuzzy logic. The torque and stator flux, have been controlled independently. The motor is started smoothly. The reference speed is generated by DC link voltage controller controlling the voltage at DC link along with the speed estimated by the feed forward term incorporating the pump affinity law. The power of PV array is maintained at maximum power point at the time of change in irradiance.

Better speed control and less torque ripples were found.

REFERENCES

[1] R. Foster, M. Ghassemi and M. Cota, Solar energy: Renewable energy and the environment, CRC Press, Taylor and francis Group, Inc. 2010.

[2] M. Kolhe, J. C. Joshi and D. P. Kothari, "Performance analysis of a directly coupled photovoltaic water-pumping system", IEEE Trans. on Energy Convers., vol. 19, no. 3, pp. 613-618, Sept. 2004.

[3] J. V. M. Caracas, G. D. C. Farias, L. F. M. Teixeira and L. A. D. S. Ribeiro, "Implementation of a high-efficiency, high-lifetime, and lowcost converter for an autonomous photovoltaic water pumping system", IEEE Trans. Ind. Appl., vol. 50, no. 1, pp. 631-641, Jan.-Feb. 2014.

[4] R. Kumar and B. Singh, " Buck-boost converter fed BLDC motor for solar PV array based water pumping, " IEEE Int. Conf. Power Electron. Drives and Energy Sys. (PEDES), 2014.

[5] Zhang Songbai, Zheng Xu, Youchun Li and Yixin Ni, "Optimization of MPPT step size in stand-alone solar pumping systems," IEEE Power Eng. Society Gen. Meeting, June 2006.

[6] H. Gonzalez, R. Rivas and T. Rodriguez, "Using an artificial neural network as a rotor resistance estimator in the indirect vector control of an induction motor," IEEE Latin Amer. Trans (Revista IEEE America Latina) , vol.6, no.2, pp.176-183, June 2008.

[7] S. K. Sahoo and T. Bhattacharya, "Field Weakening Strategy for a Vector-Controlled Induction Motor Drive Near the Six-Step Mode of Operation," IEEE Trans. Power Electron., vol. 31, no. 4, pp. 3043-3051, April 2016.

[8] T. Esram and P.L. Chapman, "Comparison of photovoltaic array maximum power point technique," IEEE Trans. Energy Convers., vol.22, no.2, pp.439-449, June 2007.

[9] F. Liu, S. Duan, F. Liu, B. Liu and Y. Kang, "A variable step size INCMPPT method for PV systems," IEEE Trans. Ind. Electron., vol. 55, no. 7, pp. 2622-2628, July 2008.

[10] M. A. Elgendy, D. J. Atkinson and B. Zahawi, "Experimental investigation of the incremental conductance maximum power point tracking algorithm at high perturbation rates," IET Renewable Power Generation, vol. 10, no. 2, pp. 133-139, Feb. 2016.

[11] A. B. Raju, S. Kanik and R. Jyoti, "Maximum efficiency operation of a single stage inverter fed induction motor PV water pumping system", Emerging Trends in Eng. And Tech. (ICETET), pp.905-910, 2008.

[12] C. Jain and B. Singh, "Single-phase single-stage multifunctional grid interfaced solar photo-voltaic system under abnormal grid conditions", IET Genr., Trans. & Distr., vol. 9, no. 10, pp. 886-894, Feb.2015.

[13] S. Shukla and B. Singh, "Single stage SPV array fed speed sensorless vector control of induction motor drive for water pumping," IEEE Int Conf. Power Electron., Intelligent Control and Energy Systems (ICPEICES), 2016, pp. 1-6, 2016.

[14] J. Titus, J. Teja, K. Hatua and K. Vasudevan, "An Improved Scheme for Extended Power Loss Ride-Through in a Voltage-Source-Inverter-Fed Vector-Controlled Induction Motor Drive Using a Loss Minimization Technique," IEEE Trans. Ind. Appl., vol. 52, no. 2, pp. 1500-1508, March-April 2016.

[15] S. A. Odhano, R. Bojoi, A. Boglietti, Ş. G. Roşu and G. Griva, "Maximum Efficiency per Torque Direct Flux Vector Control of Induction Motor Drives," IEEE Trans. Ind. Appl., vol. 51, no. 6, pp. 4415-4424, Nov.-Dec. 2015.

[16] L. An and D. D. C. Lu, "Design of a single-switch DC/DC converter for a PV-battery-powered pump system with PFM+PWM control," in IEEE Trans. Ind. Electron., vol. 62, no. 2, pp. 910-921, Feb. 2015.

[17] D. Stojić, M. Milinković, S. Veinović and I. Klasnić, "Improved stator flux estimator for speed sensorless induction motor drives," IEEE Trans. Power Electron., vol. 30, no. 4, pp. 2363-2371, April 2015.

[18] D. Casadei, G. Serra, A. Tani, L. Zarri and F. Profumo, "Performance analysis of a speed-sensorless induction motor drive based on a constant-switching-frequency DTC scheme," IEEE Trans. Ind. Appl., vol. 39, no. 2, pp. 476-484, Mar/Apr 2003.

[19] B. Singh, G.Bhuvaneswari and V.Garg, "A Novel polygon based 18- pulse AC–DC converter for vector controlled induction motor drives," IEEE Trans.Power Electron., vol.22, pp.488-497, March 2007.

[20] R. Kumar, S. Das, P.Syam and A.K. Chattopadhyay, "Review on model reference adaptive system for sensorless vector control of induction motor drives," IET Elec. Power Appl., vol.9, pp.496-511, Aug. 2015. [21] W. V. Jones, "Motor selection made easy: Choosing the right motor for centrifugal pump applications," IEEE Ind. Appl. Mag., vol. 19, no. 6, pp. 36–45, Nov./Dec. 2013.